# Probing Isotope Shifts in 103 Rh and 195 Pt NMR Spectra with Density Functional Theory

**ARTICLE** *in* THE JOURNAL OF PHYSICAL CHEMISTRY A · JULY 2013

Impact Factor: 2.69 · DOI: 10.1021/jp405453c · Source: PubMed



**3 AUTHORS**, INCLUDING:

Klaus R Koch
Stellenbosch University
**126** PUBLICATIONS **2,200** CITATIONS

SEE PROFILE

THE JOURNAL OF PHYSICAL CHEMISTRY A

Article

pubs.acs.org/JPCA

# Probing Isotope Shifts in $^{103}$Rh and $^{195}$Pt NMR Spectra with Density Functional Theory

John C. Davis,[†,‡] Michael Bühl,*[,†] and Klaus R. Koch*[,‡]

[†]School of Chemistry, University of St. Andrews, North Haugh, St. Andrews, Fife KY16 9ST, United Kingdom

[‡]Department of Chemistry and Polymer Science, University of Stellenbosch, P Bag X1, Matieland 7602, South Africa

Supporting Information

**ABSTRACT:** Zero-point vibrationally averaged ($r_g^0$) structures were computed at the PBE0/SDD/6-31G* level for the $[Pt^{35}Cl_n{}^{37}Cl_{5-n}(H_2{}^{18}O)]^-$ ($n$ = 0−5), *cis*-$Pt^{35}Cl_n{}^{37}Cl_{4-n}(H_2{}^{18}O)(H_2{}^{16}O)$ ($n$ = 0−4), *fac*-$[Pt^{35}Cl_n{}^{37}Cl_{3-n}(H_2{}^{18}O)(H_2{}^{16}O)_2]^+$ ($n$ = 0−3), $[Pt^{35}Cl_n{}^{37}Cl_{5-n}(^{16/18}OH)]^{2-}$ ($n$ = 0−5), *cis*-$[Pt^{35}Cl_n{}^{37}Cl_{4-n}(^{16/18}OH)_2]^{2-}$ ($n$ = 0−4), *fac*-$[Pt^{35}Cl_n{}^{37}Cl_{3-n}(^{16/18}OH)_3]^{2-}$ ($n$ = 0−3), *cis*-$[Pt^{35}Cl_n{}^{37}Cl_{2-n}(^{16/18}OH)_4]^{2-}$ ($n$ = 0−2), $[Pt^{35}Cl_n{}^{37}Cl_{1-n}(^{16/18}OH)_5]^{2-}$ ($n$ = 0−1), $[Rh^{35}Cl_n{}^{37}Cl_{5-n}(H_2O)]^{2-}$ ($n$ = 0−5), *cis*-$[Rh^{35}Cl_n{}^{37}Cl_{4-n}(H_2O)_2]^-$ ($n$ = 0−4), and *fac*-$Rh^{35}Cl_n{}^{37}Cl_{3-n}(H_2O)_3$ ($n$ = 0−3) isotopologues and isotopomers. Magnetic shielding constants, computed at the ZORA-SO/PW91/QZ4P/TZ2P level, were used to evaluate the corresponding $^{35/37}$Cl isotope shifts on the $^{195}$Pt and $^{103}$Rh NMR spectra, which are known experimentally. While the observed effects are reproduced reasonably well computationally in terms of qualitative trends and the overall order of magnitude (ca. 1 ppm), quantitative agreement with experiment is not yet achieved. Only small changes in M−Cl and M−O bonds upon isotopic substitution, on the order of femtometers, are necessary to produce the observed isotope shifts.

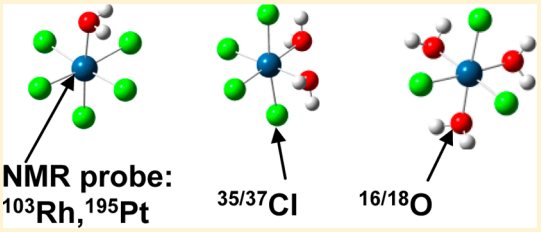


## 1. INTRODUCTION

High-resolution $^{195}$Pt NMR spectroscopy has proven to be an indispensable spectroscopic tool for the structure elucidation and characterization of numerous platinum-containing compounds in the last four decades, the topic having been extensively reviewed.[1−3] The $^{195}$Pt nucleus has been shown to be a useful NMR probe, with a range of values for chemical shifts that span 13 000 ppm, and a change of 100 ppm or more is observed when varying ligand substituents.[1]

The isotope effects on chemical shifts of transition metal nuclei in diamagnetic complexes have been reported long before the age of high-resolution NMR experiments.[4−7] These effects are very large as compared to those for other nuclei, when comparing the ranges of chemical shifts encountered.[8]

McFarlane et al.[4] illustrated the remarkable sensitivity of $\delta(^{183}W)$ toward $^{13/12}$C isotopic substitution using $^1$H-($^{183}$W), $^1$H-($^{31}$P), and $^1$H-($^{183}$W,$^{31}$P) nuclear magnetic double- and triple-resonance experiments when determining tungsten-183 chemical shifts and other parameters in tungsten(0) complexes with tertiary phosphine and cyclopentadienyl ligands. Bendall et al.[5] reported a study on $^{1/2}$H isotope shifts in $^{59}$Co NMR spectra. An isotope shift of −5 ppm per deuterium atom has been observed for the $^{59}$Co resonance of tris(ethylenediamine)-cobalt(III) chloride ($[Co(en)_3]Cl_3$) and hexaamminecobalt-(III) chloride($[Co(NH_3)_6]Cl_3$) after exchange of hydrogen for deuterium. Naumann et al.[6] reported similar isotope effects ($^1$H, $^2$H) on the $^{93}$Nb shielding of $[Et_4N][CpNb(X)(CO)_3]$ (X = H, D). An isotope shift of −6 ppm per deuterium was observed. The work on $^{51}$V NMR by Rehder[7] revealed the effect of $C^{18}O$, $^{13}$CO, $C^{18}O$, and $^2$H substitution on the $^{51}$V NMR chemical shift of $[CpV(CO)_3H]^-$ and $CpV(CO)_4$. A sizable isotope effect of −4.7 ppm is observed on going from $[CpV(CO)_3{}^1H]^-$ to $[CpV(CO)_3{}^2H]^-$. The mean isotope shift per $^{13}$CO amounts to 0.46 ppm. For $CpV(CO)_4$, the isotope shift per $C^{18}O$ substitution was found to be −0.10 ppm. In a study of water exchange rates in tetraaquaplatinum(II) and *trans*-dichloridobisaquaplatinum(II) using $H_2{}^{18}O$, Elding reported $^{16}O/^{18}O$ isotope effects induced in the $^{195}$Pt NMR of several Pt(II) complexes,[9] as well as in $[PtCl(H_2O)_5]^{3+}$ ranging up to 1.0 ppm. Sadler et al.[10] demonstrated that at relatively high magnetic fields, the $^{195}$Pt NMR resonance of the hexachloroplatinate(IV) anion could be resolved into a set of seven peaks ascribed to the $[Pt^{35/37}Cl_6]^{2-}$ species as a result of the natural $^{35}$Cl/$^{37}$Cl isotope distribution.

More Recently, Murray et al. demonstrated that in a 14.7 T magnetic field, the highly resolved 128.8 MHz $^{195}$Pt NMR resonances of $[PtCl_5(H_2O)]^-$ and *cis*-$[PtCl_4(H_2O)_2]$ show well-resolved isotope effects, which serve as unique spectroscopic "fingerprints" for the unambiguous identification of some of the aquated species derived from the hydrolysis of the $[PtCl_6]^{2-}$ anion in acidic solution, independent of the average chemical shift of these complexes.[11] It was also shown that the $^{195}$Pt NMR peaks of $[PtCl_5(H_2O)]^-$ and *cis*-$[PtCl_4(H_2O)_2]$ complexes under carefully controlled spectroscopic conditions are resolved not only according to the statistically expected isotopologues, but also in some cases due to the isotopomers

**Received:** June 3, 2013
**Revised:** July 17, 2013
**Published:** July 17, 2013

   dx.doi.org/10.1021/jp405453c | J. Phys. Chem. A 2013, 117, 8054−8064

possible for these species, depending on whether a $^{35}Cl$ or $^{37}Cl$ ion is trans to the coordinated water molecule for each isotopologue in a given complex. Isotopomers or isotopic isomers are isomers with isotopic atoms, having the same number of each isotope of each element but differing in their positions. Isotopologues are molecules that differ only in their isotopic composition. Simply, the isotopologue of a chemical species has at least one isotope of an atom different to the parent.

These remarkable isotope effects demonstrate the high sensitivity of $^{195}Pt$ shielding to very small differences in the average $^{195}Pt-^{35}Cl$ as compared to $^{195}Pt-^{37}Cl$ bond displacements in the various isotopologues and/or isotopomers possible for specific platinum complexes of a particular geometric structure. Recently, these isotope effects have been resolved for the hydroxido-chlorido complexes of Pt(IV).[12] A key feature of hydroxido-chlorido complexes is the absence of isotopomers in the experimental spectra and will be addressed in this study.

Interpretation of the origin of these isotope effects in the $^{195}Pt$ NMR signals is achieved in the context of the elegant work of Jameson et al.[13−15] whose calculation of the mean M−X bond displacements for octahedral $MX_6$ molecules including $[PtCl_6]^{2-}$ and $[PtBr_6]^{2-}$ using L-tensor and Bartell methods with anharmonic force fields showed that the expected nuclear shielding changes in M (and where appropriate X) as a result of isotope replacement (and/or temperature effects) should be directly correlated to the mean M−L bond displacement. Consequently, a direct proportionality between the isotope induced shielding of, in this case, $^{195}Pt$ and the mass factor $(m' - m)/m'$ may be expected on $^{37}Cl$ for $^{35}Cl$ substitution. In general, as a heavier $^{37}Cl^-$ replaces a $^{35}Cl^-$ ion in the coordination sphere, increased shielding of the $^{195}Pt$ is observed for a given isotopologue of a given species, as a result of some slight Pt−Cl bond contraction; the extent of this effect measured by $\Delta\delta^{195}Pt$ depends on the overall number of coordinated $Cl^-$ ions and the structure of the complex, but there appears to be no obvious/simple correlation between the magnitude of the $\Delta\delta^{195}Pt$ value and $n$ in $[PtCl_n(H_2O)_{6-n}]^{4-n}$ ($n$ = 2−5). It is noteworthy that the average chemical shift difference per $^{37}Cl$, that is, between the individually resolved isotopologue resonances, is only $\Delta\delta^{195}Pt$ = 0.22 ppm (ca. 28 Hz on a 128.8 MHz spectrometer).

More recently, it has been observed that when $^{18}O$-enriched water is used as solvent, additional signals appear, which are ascribed to $H_2{}^{16/18}O$ isotopologues and isotopomers.[16]

Quantum-chemical computation of transition-metal chemical shifts is a stronghold of density functional theory (DFT),[17] and the advent of relativistic methods such as the zero-order regular approximation (ZORA) has made $^{195}Pt$ NMR parameters amenable to computational study.[18−20]

Most of these calculations employ static equilibrium structures, which are independent of atomic masses. Using zero-point vibrationally averaged structures, isotope effects on $^{59}Co$ chemical shifts have been reproduced and rationalized computationally.[21,22] In a cobaloxime[21] and the hexamine cobalt(III) complex,[22] the observed $^1H/^2H$ shifts on the order of ca. 50−100 ppm could be traced back to small changes in the Co−N bonds, on the order of 0.001−0.006 Å, upon isotopic substitution. Because of their much smaller magnitude, typically 1 ppm or less,[23] the above-mentioned isotope effects on $^{195}Pt$ shifts pose a much bigger challenge to theory.

In our previous paper,[24] we have calculated such zero-point corrections to the gas-phase geometries of $[Pt^{35}Cl_6]^{2-}$ and $[Pt^{37}Cl_6]^{2-}$, for the $[Pt^{35}Cl_n{}^{37}Cl_{5-n}(H_2{}^{16}O)]^-$ (**1**, $n$ = 0−5), *cis*-$Pt^{35}Cl_n{}^{37}Cl_{4-n}(H_2{}^{16}O)_2$ (**2**, $n$ = 0−4), and *fac*-$[Pt^{35}Cl_n{}^{37}Cl_{3-n}(H_2{}^{16}O)_3]^+$ (**3**, $n$ = 0−3) isotopologues and isotopomers. The $^{35/37}Cl$ isotope shifts on $\delta^{195}Pt$ evaluated for these zero-point corrected (effective) geometries were found to qualitatively reproduce the observed trends and were found to be useful for the interpretation of the latter.

This computational protocol is now extended to $[Pt^{35}Cl_n{}^{37}Cl_{5-n}(H_2{}^{18}O)]^-$ ($n$ = 0−5), *cis*-$Pt^{35}Cl_n{}^{37}Cl_{4-n}(H_2{}^{18}O)(H_2{}^{16}O)$ ($n$ = 0−4), *fac*-$[Pt^{35}Cl_n{}^{37}Cl_{3-n}(H_2{}^{18}O)(H_2{}^{16}O)_2]^+$ ($n$ = 0−3), $[Pt^{35}Cl_n{}^{37}Cl_{5-n}(OH)]^{2-}$ ($n$ = 0−5), *cis*-$[Pt^{35}Cl_n{}^{37}Cl_{4-n}(OH)_2]^{2-}$ ($n$ = 0−4), *fac*-$[Pt^{35}Cl_n{}^{37}Cl_{3-n}(OH)_3]^{2-}$ ($n$ = 0−3), *cis*-$[Pt^{35}Cl_n{}^{37}Cl_{2-n}(OH)_4]^{2-}$ ($n$ = 0−2), and $[Pt^{35}Cl_n{}^{37}Cl_{1-n}(OH)_5]^{2-}$ ($n$ = 0−1), as well as their $^{16/18}OH$ isotopologues. For the aquo complexes, large solvation effects were apparent, but were found difficult to include at present.[24] It is known that immersion in a polar solvent can reinforce metal−water bonds, probably due to cooperative polarization effects.[25] In the gas phase, DFT tends to underestimate metal−ligand bond strengths, in particular in dative bonds involving water.[26] The consequences on the computed isotope shifts are yet unknown.

While the hydroxido complexes are expected to interact more strongly with the solvent than the aquo species due to their higher charge (−2), the fact that hydroxido and chlorido ligands have the same charge could mean that solvation affects the bonds rather more uniformly in the hydroxido than in the aquo complexes. Thus, the protocol for the gas-phase calculations presented previously[24] could still be a good approximation to the situation in solution, if effective error cancelation occurs, a possibility that will be explored in this Article.

Recent developments show that at high magnetic fields with carefully controlled solution temperatures, the 19.11 MHz $^{103}Rh$ NMR[27] signals of the series of $[RhCl_n(H_2O)_{6-n}]^{3-n}$ ($n$ = 3−6) complexes in equilibrated hydrochloric acid solutions are also well-resolved into a distinctive fine-structure due to $^{35}Cl/^{37}Cl$ isotopologue and isotopomer effects, resulting in a unique NMR fingerprint.[28]

We now extend our computational protocol to $[Rh^{35}Cl_n{}^{37}Cl_{5-n}(H_2O)]^{2-}$ ($n$ = 0−5), *cis*-$[Rh^{35}Cl_n{}^{37}Cl_{4-n}(H_2O)_2]^-$ ($n$ = 0−4), and *fac*-$Rh^{35}Cl_n{}^{37}Cl_{3-n}(H_2O)_3$ ($n$ = 0−3) isotopologues and isotopomers.

The monoaquo Rh(III) complex has a higher charge (−2) than the Pt(IV) aquo-complexes (up to ±1), which might lead to increased interactions with the solvent. With the same kind of trans influence operative in both Pt(IV) and Rh(III) series, the importance of the overall charge on the computed isotope shifts can now be assessed. Investigating these species in comparison to Pt(IV) aquo complexes is expected to inform on the reason why isotopomers are resolved in some cases, but not always.

## 2. COMPUTATIONAL DETAILS

The same protocol as in our previous study[24] was applied. Geometries were fully optimized using at the PBE0/ECP1 level, that is, employing the hybrid variant of the PBE


dx.doi.org/10.1021/jp405453c | J. Phys. Chem. A 2013, 117, 8054−8064

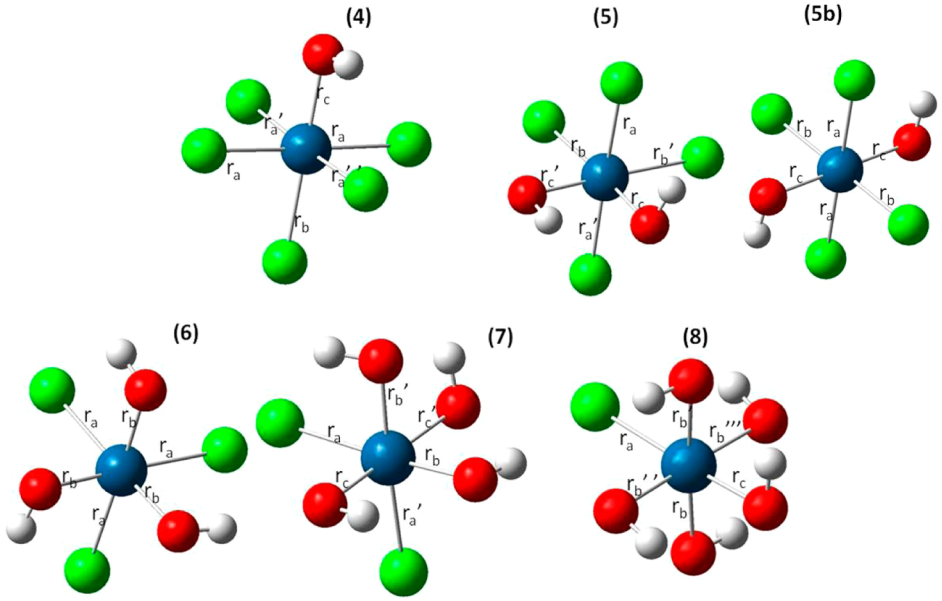


**Figure 1.** Optimized structures of (**4**) $[PtCl_5(OH)]^{2-}$, (**5**) *cis*-$[PtCl_4(OH)_2]^{2-}$, (**6**) *fac*-$[PtCl_3(OH)_3]^{2-}$, (**7**) *cis*-$[PtCl_2(OH)_4]^{2-}$, (**8**) $[PtCl(OH)_5]^{2-}$, and (**5b**) *trans*-$[PtCl_4(OH)_2]^{2-}$.

functional,[29,30] the Stuttgart−-Dresden relativistic effective core potential (SDD ECP) along with its [6s5p3d] valence basis on Pt and Rh,[31] and 6-31G* basis[32−34] elsewhere. This combination of functional and basis sets has performed very well for the description of bond distances between third-row transition metals and their ligands.[35] Unless otherwise noted, tight optimization criteria and a fine integration grid were employed (opt=tight, grid=finegrid options in Gaussian).

Effective geometries, $r_g^0$ at 0 K, were constructed in a perturbational approach from the equilibrium geometries $r_e$, the (mass-dependent) harmonic frequencies $\omega_e$, and the cubic force field $V^{(3)}$ (for details, see refs 36−40).[41,42]

$$r_{g,j}{}^0 = r_{e,j} + \Delta r_{g,j}{}^0 = r_{e,j} - \frac{1}{4\omega_{e,j}{}^2}\sum_m \frac{V^{(3)}_{e,jmm}}{\omega_{e,m}} \quad (1)$$

These calculations were performed using the Gaussian 09 suite of programs.[43]

For $r_e$ and $r_g^0$ geometries of each isotopic substitution, $^{195}$Pt and $^{103}$Rh shielding tensors were computed at the relativistic spin−orbit ZORA level, using the GGA PW91[44,45] functional, together with an all-electron quadruple-ζ plus polarization function (QZ4P) basis set on Pt and Rh and polarized valence triple-ζ basis sets (TZP) on Cl and $H_2O$. The integration precision parameter was set to 10.0. These calculations employed the ADF2010.02 program.[46]

Selected complexes were reoptimized with the CPCM method,[47,48] the equivalent of the conductor-like screening model (COSMO), as implemented in Gaussian 09, together with the parameters of water. Magnetic shieldings of these complexes were computed using the COSMO method[49] as implemented in ADF2010.02.

This level of theory performed well for the calculation of chemical shifts for various heavy metal complexes. For example, Autschbach et al.[18−20] reported $^{195}$Pt and $^{205}$Tl NMR chemical shifts of the complexes $[(NC)_5Pt-Tl(CN)_n]^{n-}$ $n = 0-3$, and of the related system $[(NC)_5Pt-Tl-Pt(CN)_5]^{3-}$ calculated at this level. Koch et al.[50] reported reasonably accurate $^{195}$Pt chemical shifts of a series of octahedral $[PtX_{6-n}Y_n]^{2-}$ complexes for X = Cl, Br, F, I. Although $\delta(^{103}Rh)$ can be calculated at a nonrelativistic level,[17,51] for consistency with the $^{195}$Pt chemical shift calculations, ZORA-SO is also applied, which has been shown to work well also for $^{103}$Rh.[52]

## 3. RESULTS AND DISCUSSION

**3.1. $^{35/37}$Cl Isotope Effects in $[PtCl_n(OH)_{6-n}]^{2-}$ ($n = 1-5$) Complexes.** DFT geometry optimizations were performed to calculate the ground-state equilibrium and zero-point averaged structures in the gas phase of all of the relevant complexes. These structures were then used in the theoretical determination of the $^{195}$Pt shielding tensors. Figure 1 shows the optimized geometries of $[PtCl_5(OH)]^{2-}$ (**4**), *cis*-$[PtCl_4(OH)_2]^{2-}$ (**5**), *fac*-$[PtCl_3(OH)_3]^{2-}$ (**6**), *cis*-$[PtCl_2(OH)_4]^{2-}$ (**7**), and $[PtCl(OH)_5]^{2-}$ (**8**).

In all minima, the OH bonds are essentially eclipsing other Pt−O or Pt−Cl bonds, arguably due to intramolecular OH···X interactions driven by electrostatics (for proper hydrogen bonds, the bond angles would be too small). No extensive conformational searches were undertaken, except for *cis*-$[PtCl_4(OH)_2]^{2-}$, as discussed below.

The Pt−Cl bonds trans to a hydroxido group are longer than those in a cis position, in agreement with observations from X-ray crystallography for **4**[53] and **5b**[54] (compare $r_a$ vs $r_b$ in Table S1 in the Supporting Information). This is mainly due to the larger trans influence of $OH^-$ relative to that of $Cl^-$.[55] For the aquo complexes, the trans influence of $Cl^-$ was larger than that of $H_2O$, leading to a shorter Pt−Cl bond trans to a coordinated $H_2O$.

The Pt−$^{35}$Cl bonds are longer relative to Pt−$^{37}$Cl bonds as expected from the effect of anharmonicity as seen in Table S2 in the Supporting Information. A similar trend was found for the Pt−O bonds in Table S3 in the Supporting Information, where the Pt−$^{16}$O bonds extend further in space than the corresponding Pt−$^{18}$O bond. Note that the zero-point corrections to the eqilibrium Pt−Cl distances are of the same order of magnitude as for the aquo complexes,[24] ca. 0.5 pm (Table S1, Supporting Information). The same is found for the


dx.doi.org/10.1021/jp405453c | J. Phys. Chem. A 2013, 117, 8054−8064

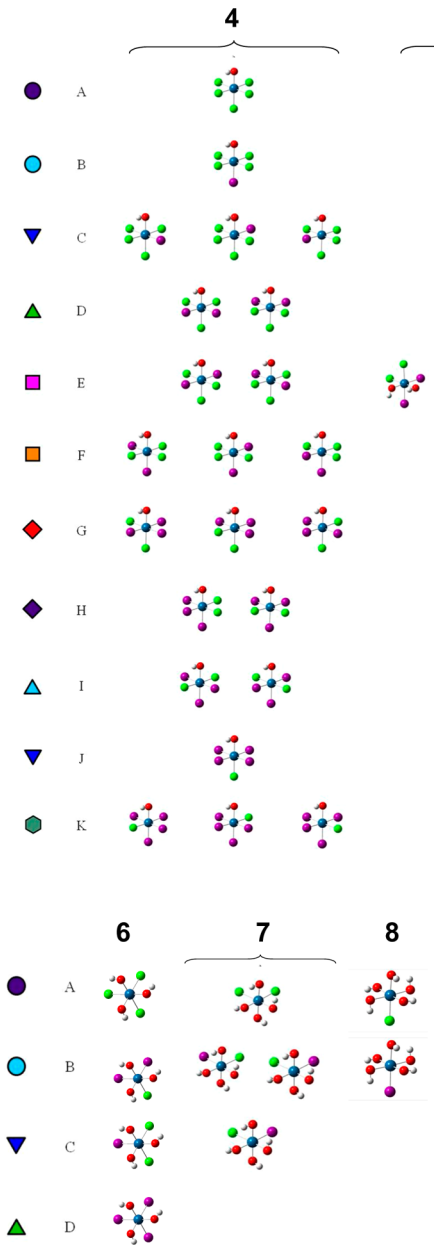


**Figure 2.** Isotopomers of (**4**) $[PtCl_5(OH)]^{2-}$, (**5**) *cis*-$[PtCl_4(OH)_2]^{2-}$, (**6**) *fac*-$[PtCl_3(OH)_3]^{2-}$, (**7**) *cis*-$[PtCl_2(OH)_4]^{2-}$, (**8**) $[PtCl(OH)_5]^{2-}$, together with the labeling scheme adopted in the following figures. Color code: $^{35}Cl$ green, $^{37}Cl$ purple.

difference between the Pt−$^{35}$Cl and Pt−$^{37}$Cl bonds, up to ca. 40 fm (Table S2, Supporting Information).

Although it is the trans isomer of $[PtCl_4(OH)_2]^{2-}$ that is found to crystallize with particular counterions,[54] *cis*-$[PtCl_4(OH)_2]^{2-}$ is calculated to be more stable by 0.3 kcal/mol. For the purpose of this study, only (**5**) *cis*-$[PtCl_4(OH)_2]^{2-}$ was included in the isotope shift calculations.

All possible $^{35/37}$Cl isotopomers were calculated in the gas phase for complexes **4**−**8**. The resulting vibrationally averaged structures were used as inputs for relativistic calculations of isotropic magnetic shielding constants at the ZORA-SO/PW91/QZ4P/TZ2P level. To compare with experiment, isotope shifts $\Delta\delta$ were calculated relative to the corresponding all-$^{35}$Cl isotopologue set to $\delta = 0$. The resulting isotopomers are displayed in Figure 2.

Many of the static isotopomer structures can be interconverted through simple OH rotation about the Pt−O bonds, processes that are expected to occur very rapidly on the NMR time scale as discussed below. Thus, it is reasonable to assume that those isotopomers that are grouped together in the legends will only show a single NMR signal, and their computed shielding constants were averaged accordingly.

In complex **5**, there is one OH···O and one OH···Cl contact. Two OH···Cl contacts can be enforced by imposing $C_2$ symmetry. This stationary point is not a minimum, but rather a transition state (with one imaginary frequency) connecting two degenerate rotamers of the $C_1$-symmetric minimum, as shown in the energy profile below.

The energy barrier for this interconversion shown in Figure 3 is 1.2 kcal mol$^{-1}$, which is readily overcome on the time scale of

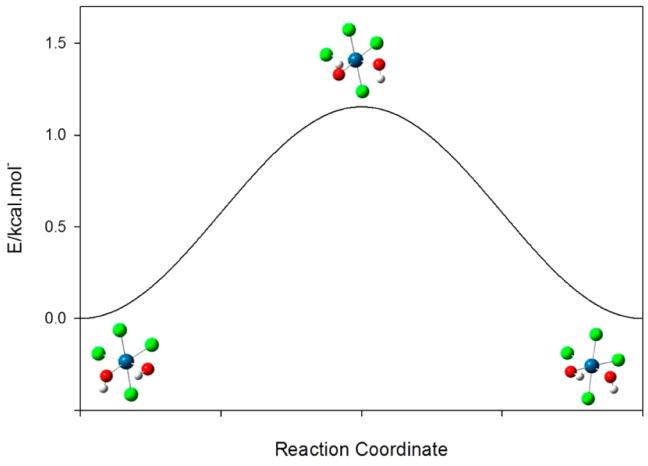


**Figure 3.** Energy profile of *cis*-$[PtCl_4(OH)_2]^{2-}$. The minima obtained interconvert via the transition state shown at the maximum.

the NMR experiments under standard conditions in solution (typical barriers that can be "frozen out" in variable-temperature NMR are on the order of ∼10 kcal mol$^{-1}$, the precise value depending on the shift difference and the actual rate constant[56]). Thus, it is indeed likely that the OH groups rotate spontaneously and rapidly about the Pt−O bonds on the NMR time-scale.[56]

For complex **4**, the resulting shielding constants and the corresponding experimental isotope shifts are collected (Table S4 in the Supporting Information) and, after conversion of the computed shieldings into relative shifts, plotted against each other in Figure 4. The sign of the experimental isotope shifts has been reversed, so that they appear in the same sequence as in a conventional NMR spectrum.

The overall observed trends as well as the overall order of magnitude of the isotope shifts are reasonably well reproduced by our computational protocol. As found for the aquo complexes in the previous paper, however,[24] there are quantitative discrepancies, apparent in a noticeable scatter of the data and a typically overestimated slope of the $\Delta\sigma_{calc}$ versus $\Delta\delta_{exp}$ data. It is unclear at present whether these discrepancies are due to residual numerical errors in the computations, deficiencies of the overall model (e.g., the neglect of thermal effects beyond the zero-point corrections), or missing solvation.

Overall, however, this result is consistent with what has been found for the aquo complexes,[24] further validating our model. The divergence of the calculated shielding of the isotopomers of **4**, labeled in Figure 4 as (B,C), (D,E,F), (G,H,I), and (J,K),


dx.doi.org/10.1021/jp405453c | J. Phys. Chem. A 2013, 117, 8054−8064

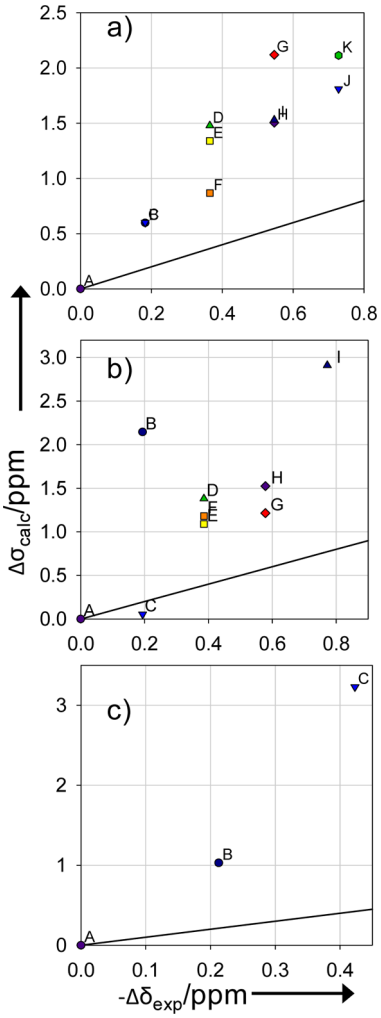


**Figure 4.** Calculated shielding differences versus negative experimental $^{35/37}$Cl isotope shifts of the isotopomers of Figure 2, including the ideal line with unity slope. (a) $[PtCl_5(OH)]^{2-}$ (**4**), (b) *cis*-$[PtCl_4(OH)_2]^{2-}$ (**5**), and (c) *cis*-$[PtCl_2(OH)_4]^{2-}$ (**7**).

and **5** labeled as (B,C), (D,E,F) and (H,G), will be discussed in section 3.5.

**3.2. $^{16/18}$O Isotope Effects in $[PtCl_n(H_2O)]^{4-n}$ ($n$ = 3−5) and $[PtCl_n(OH)_{6-n}]^{2-}$ ($n$ = 1−5) Complexes.** So far, only $^{35/37}$Cl isotopic substitutions have been considered, which arise from the natural distribution of these two isotopes. Recently, it has been observed that when $^{18}$O-enriched water is used as solvent, the characteristic $^{195}$Pt fingerprints from the $^{35/37}$Cl substitution patterns are split into two more sets of signals, which are ascribed to $^{16/18}$O isotopologues and isotopomers.[16] We have now also computed these $^{16/18}$O isotope effects. We begin our discussion with the aquo complexes **1**−**3** (Figure 5). We note in passing that as with **5**, cis/trans isomerism could be possible for the bis(aquo) complex **2**. However, *trans*-$PtCl_4(H_2O)_2$ is computed 6.1 kcal/mol higher in energy than the cis isomer (PBE0 level), in line with the observation of the latter in the solid[57] (cf., Table S6 in the Supporting Information). Also, the observation of separate isotopomers for the singly and triply substituted species (e.g., B and C in Figures 5 and 6, middle) would make the trans form an unlikely candidate for the experimentally observed spectrum. Thus, only the cis form has been considered in the computations.

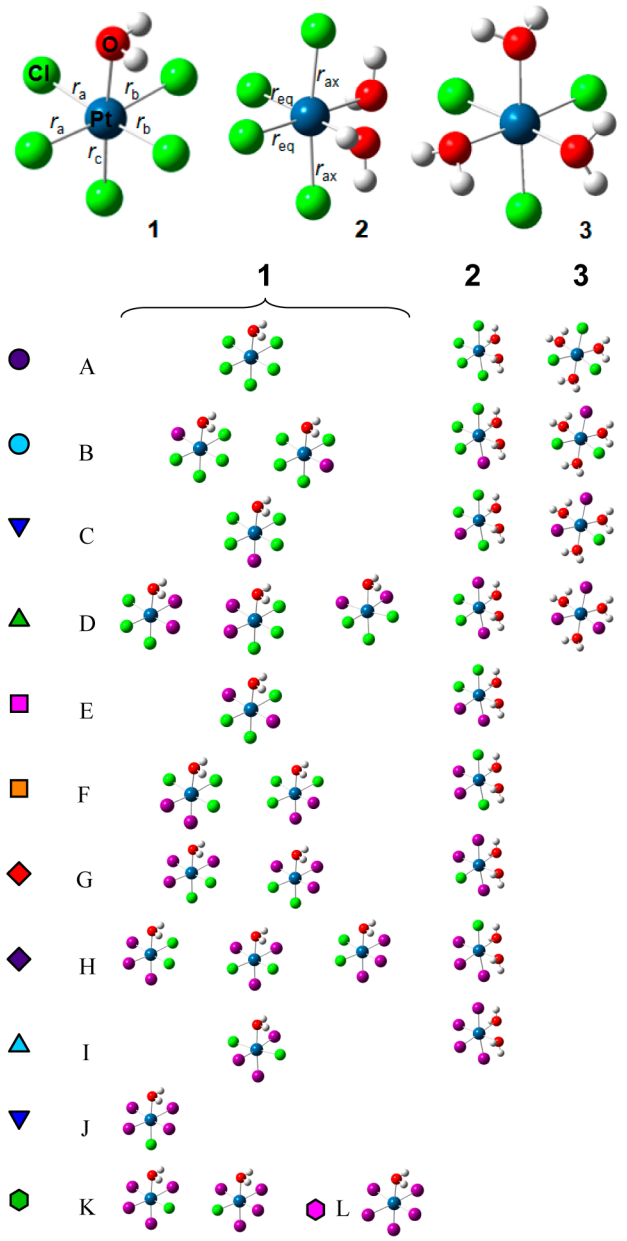


**Figure 5.** Top: Optimized structures of $[PtCl_5(H_2O)]^-$ (**1**), *cis*-$PtCl_4(H_2O)_2$ (**2**), and *fac*-$[PtCl_3(H_2O)_3]^+$ (**3**). Bottom: Isotopomers with the labeling scheme adopted in the following figures. Color code: $^{35}$Cl green, $^{37}$Cl purple.

The $^{35/37}$Cl isotope effects for the $H_2{}^{16}O$ isotopologues had been reported previously.[24] The computed $^{35/37}$Cl isotope shifts for the corresponding $^{18}$O isotopomers are plotted against experiment in Figure 6. The same patterns as for the parent $^{16}$O complexes were expected (as found experimentally);[16] however, noticeably different results were obtained. For instance, for complex **1** the overall computed range, that is, the difference between isotopologues A and K (or J), increases from ca. 1.3 ppm with $H_2{}^{16}O$[24] to ca. 1.8 ppm with $H_2{}^{18}O$ (Figure 6a), as compared to ca. 0.8 ppm observed for both. Experimentally, substitution of $^{16}$O for $^{18}$O in each isotopomer of **1** affords a rather constant upfield shift of $\Delta\delta(^{195}Pt) \approx 0.7 \pm 0.05$ ppm. The variation in the computed $\Delta\sigma$ values is much larger and rather unsystematic, ranging from $\Delta\sigma \approx +0.8$ ppm to ∼−0.5 ppm (see Figure S1 in the Supporting Information). It


dx.doi.org/10.1021/jp405453c | J. Phys. Chem. A 2013, 117, 8054−8064

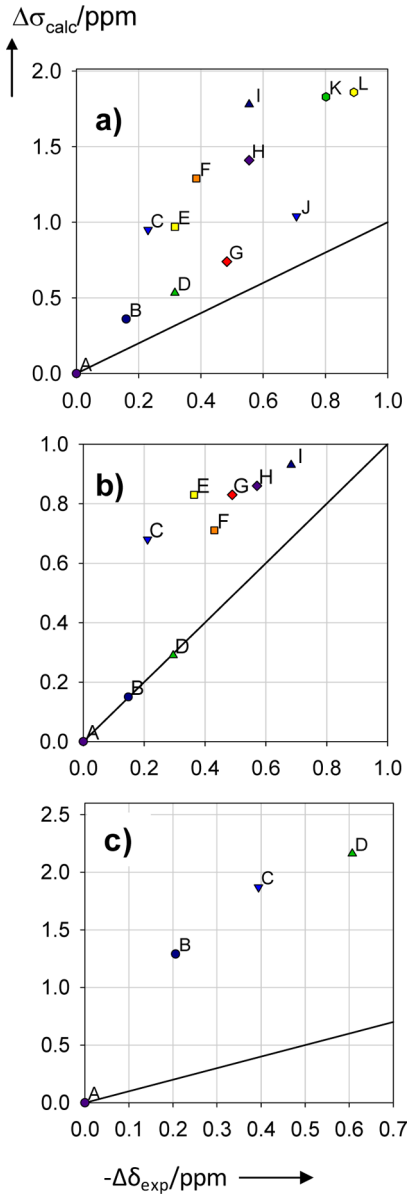


**Figure 6.** Calculated shielding differences versus negative experimental $^{35/37}$Cl isotope shifts of the isotopomers of Figure 5, including the ideal line with unity slope. (a) $[PtCl_5(H_2{}^{18}O)]^-$; (b) *cis*-$PtCl_4(H_2{}^{16}O)(H_2{}^{18}O)$; (c) *fac*-$[PtCl_3(H_2{}^{18}O)(H_2{}^{16}O)_2]^+$.

appears that the sensitivity of the Pt−O bond length toward isotopic substitution is not very well captured by the present approach.

The origin of this large discrepancy is not fully clear at present, but there are reasons to assume that solvation effects, so far neglected in our approach, can be decisive. In many computational studies of transition-metal aquo complexes, it has been found that the M−$OH_2$ distances can decrease appreciably on going from the gas phase into an aqueous solution.[25] Apparently, the trans influence, which is prevalent among Pt(IV) and Pt(II) complexes[55](see optimized and measured Pt−Cl and Pt−O distances in Tables S6 and S7, Supporting Information), is somewhat attenuated in solution, and the water ligands are bound too weakly in the gas phase. In fact, remarkably large vibrational corrections $\Delta r_g{}^0 \approx 0.01$ Å are obtained for the Pt−O bonds in the gas phase (Table S7, Supporting Information), indicative of rather anharmonic, shallow stretching potentials. As expected, the Pt−$^{16}$O bonds are longer than the Pt−$^{18}$O bonds (Table S7, Supporting Information), but it appears difficult to model the sensitivity of the Pt−O bond length toward isotopic substitution quantitatively.

The same is apparent for the hydroxido-complexes discussed above: for example, experimentally for $[Pt^{35/37}Cl_5(OH)]^{2-}$ (**4**), substitution of $^{16}$O for $^{18}$O in each isotopomer affords a rather constant upfield shift of $\Delta\delta(^{195}Pt) \approx 0.7 \pm 0.05$ ppm.[16] The variation in the computed $\Delta\sigma$ values is much larger and the isotopomers are not grouped together, ranging from $\Delta\sigma \approx +0.8$ ppm to ∼−0.04 ppm (see Figure S2 in the Supporting Information) similar to the aquo complexes (see Figure S1 in the Supporting Information). Upon moving from the $^{16}$O to the $^{18}$O species, the deviations from experiment descrease slightly, in particular for complexes **5** and **7** (compare Figures 4 and 7). For **5**, there is somewhat less scatter and deviation from the ideal line. The isotope shifts of isotopomers B and C are

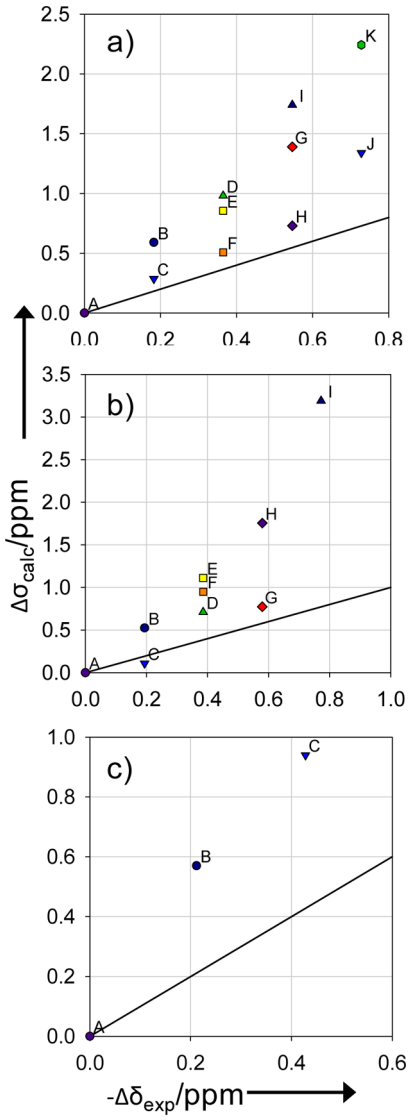


**Figure 7.** Calculated shielding differences versus negative experimental $^{35/37}$Cl isotope shifts of the isotopomers of Figure 2, including the ideal line with unity slope. (a) $[PtCl_5(^{18}OH)]^{2-}$ (**4**), (b) *cis*-$[PtCl_4(^{18}OH)_2]^{2-}$ (**5**), and (c) *cis*-$[PtCl_2(^{18}OH)_4]^{2-}$ (**7**).


dx.doi.org/10.1021/jp405453c | J. Phys. Chem. A 2013, 117, 8054−8064

also closer together, consistent with what has been found experimentally.

Overall, however, the agreement with experiment is less pronounced for the hydroxido species (**4**–**8**) than for the aquo complexes (**1**–**3**), as can be seen by the overestimation of the slope of the calculated shielding differences versus experimental $^{35/37}$Cl isotope shifts plots (compare, for instance, Figures 6 and 7).

**3.3. $^{35/37}$Cl Isotope Effects in $[RhCl_n(H_2O)_{6-n}]^{3-n}$ ($n$ = 3–5) Complexes.** We have applied our protocol to the corresponding isotope effects on $\delta(^{103}Rh)$ in $[Rh^{35}Cl_n{}^{37}Cl_{5-n}(H_2O)]^{2-}$ (**9**, $n$ = 0–5), *cis*-$[Rh^{35}Cl_n{}^{37}Cl_{4-n}(H_2O)_2]^{-}$ (**10**, $n$ = 0–4), and *fac*-$Rh^{35}Cl_n{}^{37}Cl_{3-n}(H_2O)_3$ (**11**, $n$ = 0–3). The geometries for these complexes are similar to those of the Pt-aquo complexes **1**–**3** (top of Figure 5).[58] The equilibrium bond lengths are longer (by ∼0.03 Å) for Rh complexes, however. The zero-point corrections for the metal–ligand bond distances in the Rh (**9**–**11**) and Pt-aquo complexes (**1**–**3**) are very similar (compare Tables S6, S7, and S9 in the Supporting Information). Isotope shifts $\Delta\delta$ were calculated assuming rapid $H_2O$ rotation about the Rh–O bonds and using the same labeling scheme as for the Pt congeners (Figure 5). The resulting shielding constants and the corresponding experimental isotope shifts are collected in Table S10 in the Supporting Information and, after conversion of the computed shieldings into relative shifts, plotted against each other in Figure S3 (Supporting Information). For complex **11**, the resulting plot is reproduced in Figure 8.

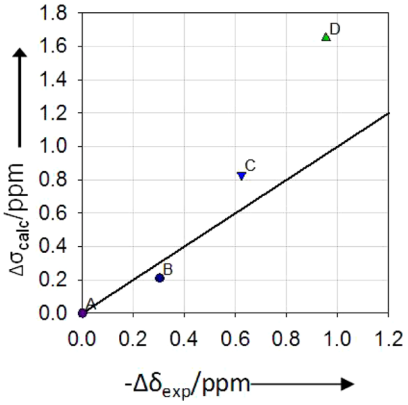


**Figure 8.** Calculated shielding differences versus negative experimental[28] (**11**) *fac*-$Rh^{35}Cl_n{}^{37}Cl_{3-n}(H_2O)_3$. The labeling scheme is the same as in Figure 5.

As compared to the Pt-aquo complexes, there is much more scatter that may be due to the "softer" nature of the Rh–L (L = $H_2O$, $Cl^-$) bonds, which enhance solvent interaction. The errors are more pronounced with complexes C, F, H, and I for **9** (Figure S3, top, Supporting Information) and F, G, and H for **10** (Figure S3, middle, Supporting Information). Interestingly, these are the isotopomers with a $^{37}$Cl trans to a $H_2O$ ligand.

Overall, it appears that the errors in the computations increase with (absolute) charge: neutral complexes are described the best (**2**, **11**, cf., Figures 6b and 8), followed by singly charged species (**1**, **3**, **10**, cf., Figures 6a,c and S3, middle, Supporting Information), with the largest deviations found for dianionics **4**–**9**. This could point to missing solvation as the key factor. For **9**, this is probably compounded by the softer nature of the M–$OH_2$ bond, as compared to the M–OH bond in dianionic **4**–**8**.

**3.4. Shielding/Bond-Length Derivatives.** It has been shown that the bond-length changes due to zero-point vibrations are the dominant factors influencing the $^{35/37}$Cl isotope shifts in **1**–**3**.[24] To confirm the same for the hydroxido-complexes **4**–**8**, we used representative shielding/bond-length derivatives $\partial\sigma_{Pt}/\partial r_{PtX}$ (X = O and Cl), together with the computed zero-point corrections for each bond length, $i$ ($\Delta r_g^0$ in eq 2) and the shieldings for the equilibrium geometry, $\sigma_e$, to estimate effective shieldings at 0 K, $\sigma_{g,est}{}^0$, according to eq 2.

$$\sigma_{g,est}{}^0 = \sigma_e + \sum_{i=1}^{6} \Delta r_{g,i}{}^0 \frac{\partial \sigma Pt}{\partial r_{PtX,i}} \qquad (2)$$

These estimated shieldings can then be compared to the actual effective shieldings computed for the vibrationally averaged structure. Pt–Cl and Pt–O shielding/bond-length derivatives have been evaluated for **4**–**8** by rigid scans of the different Pt–Cl and Pt–O bonds about their equilibrium values. The resulting $\partial\sigma_{Pt}/\partial r_{PtCl}$ and $\partial\sigma_{Pt}/\partial r_{PtO}$ values are listed in Table S11 in the Supporting Information. Figure 9 shows the resulting estimated $^{37/35}$Cl isotope effects on the $^{195}$Pt shieldings of **4**–**8**, plotted versus the actual computed values.

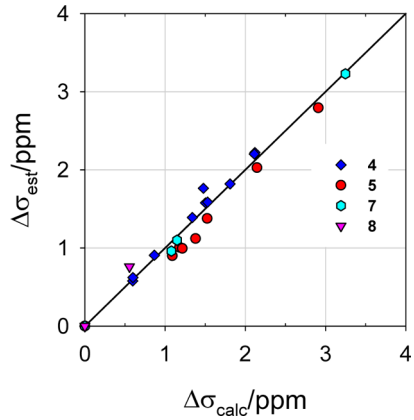


**Figure 9.** Shielding differences in $^{35/37}$Cl isotopomers of **4**–**8**, estimated from eq 2, versus actual computation from $r_g^0$ geometries, including the line with unity slope.

Both span and sequence of the $\Delta\sigma$ values are described rather well by the increment method. This result further substantiates our underlying model, that the dominant factor influencing the isotope shifts is the bond-length changes due to zero-point vibrations.

Similarly, Rh–Cl and Rh–O shielding/bond-length derivatives have been evaluated for **9**–**11** through rigid scans of the Rh–Cl and Rh–O bonds. The resulting $\partial\sigma_{Rh}/\partial r_{RhCl}$ and $\partial\sigma_{Rh}/\partial r_{RhO}$ values are listed in Table S12 (Supporting Information), and the estimated $^{37/35}$Cl isotope effects on the $^{103}$Rh shieldings are plotted versus the actual computed values in Figure S4 (Supporting Information).

As compared to the Pt-aquo complexes **1**–**3** (see the Supporting Information of ref 24), the shielding/bond-length derivatives are consistently larger for the Rh congeners **9**–**11** (typically by a factor of 1.5). This finding is consistent with the observation that the total span of the $^{35/37}$Cl isotope effects in these systems is larger for $\delta(^{103}Rh)$, ca. 1.2 ppm,[28] than for $\delta(^{195}Pt)$, ca. 0.7 ppm.[11,16] This enhanced sensitivity of the metal


dx.doi.org/10.1021/jp405453c | J. Phys. Chem. A 2013, 117, 8054–8064

shielding to the metal−ligand distances in case of the Rh(III) complexes may contribute to the larger errors in the computed isotope shifts as compared to the Pt(IV) species, although the order of magnitude of the calculated isotope shifts can still be traced back to that in zero-point corrections to the bond distances (Figure S4 in the Supporting Information). Larger discrepancies are found for complexes C, F, H, and I for **9**, as before these are the isotopomers with a $^{37}$Cl trans to a $H_2O$ ligand. With −6500 ppm/Å, the Rh−O bond in this complex is also the largest shielding/bond-length derivative among all species **1**−**11**.

**3.5. Solvation Effects and Isotopomers.** As had been shown for complex **2**, a simple polarizable continuum model (PCM) is inappropriate to evaluate solvent effects on the isotope shifts under scrutiny, because of apparent numerical instabilities during evaluation of the cubic force field $V^{(3)}$ in eq 1.[24] Microsolvation in a $[PtCl_5(H_2O)]^-\cdot 2H_2O$ cluster was shown to have a noticeable impact on the computed isotope shifts, without improving quantitative accuracy.[24] To probe the effect of the overall charge of the complex, we have now optimized the corresponding $[RhCl_5(H_2O)]^{2-}\cdot 2H_2O$ cluster, placing the two extra water molecules such that they each accept an $OH\cdots OH_2$ hydrogen bond from the coordinated water ligand (Figure 10, top).

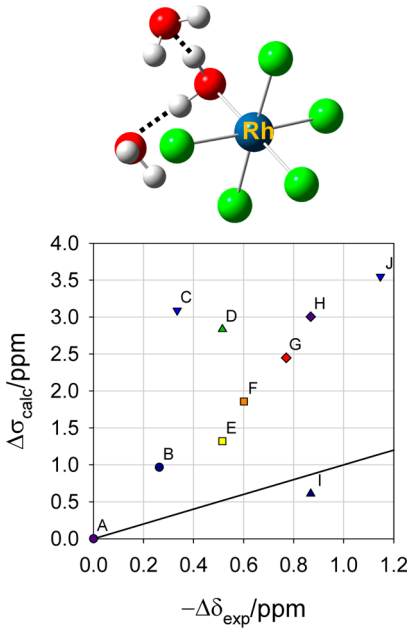


**Figure 10.** Calculated shielding differences versus negative experimental $^{35/37}$Cl isotope shifts of the isotopomers of $[RhCl_5(H_2O)]^{2-}\cdot 2H_2O$, including the ideal line with unity slope.

On going from pristine **9** to $[RhCl_5(H_2O)]^-\cdot 2H_2O$, the equilibrium Rh−O bond distance decreases from 2.190 to 2.148 Å, similar to what is found in a continuum for (e.g., decrease from 2.1265 to 2.1052 Å for **11**). At the same time, the zero-point correction for the Rh−O distance changes from $\Delta r_g^0$ = 0.015 Å (Table S9, Supporting Information) to 0.013 Å upon microsolvation, consistent with a stronger, stiffer bond.

As compared to pristine **9** (Figure S3, top, Supporting Information), there is visible improvement in the computed $^{35/37}$Cl isotope shifts for the microsolvated complex (Figure 10), that is, less scatter and values somewhat closer to experiment. The slope of the linear trend improves noticeably (from roughly 5 to 3), but is still much higher than unity. It is likely that the full solvation sphere would be needed for better accuracy, which is, however, prohibitively expensive at this point.

To probe whether microsolvation could also improve the description of the dianionic Pt hydroxido-complexes, an explicit $H_2O$ was added to $[PtCl_5(OH)]^{2-}$ (**4**). As documented in Figure S7 (Supporting Information), however, no improvement was found over the results for the pristine complex shown in Figure 4a. Apparently, in our microsolvated complexes, the distinction between cis and trans chloride ligands is overestimated to a large extent, consistent with the fact that only the former interact with the extra water molecules, not the latter. Many more water molecules would have to be added, eventually necessitating a dynamical description (CPMD or QM/MM) and exceeding the scope of this study.[59−61]

The main difference seen in the experimental $^{195}$Pt NMR spectra between the aquo complexes **1**−**3** and the hydroxido-complexes **4**−**8** is the absence of isotopomers for the latter. For instance, while two distinct signals can be resolved for $[Pt^{35}Cl_4{}^{37}Cl(H_2O)]^-$,[11] which can be assigned to complexes B and C (cf., the labeling of the corresponding Rh complexes in Figure 5), only one signal is observed for the deprotonated analogue $[Pt^{35}Cl_4{}^{37}Cl(OH)]^{2-}$;[12] that is, the signals for complexes B and C (Figure 2) are not resolved.

The failure to resolve isotopomers could in principle be due to rapid (on the NMR time-scale) interconversion between them. This possibility (i.e., conformational nonrigidity) is highly unlikely, however, because it would be very difficult to explain why the hydroxido-complex should be fluxional whereas the corresponding aquo species would not be. An associate exchange mechanism involving more fluxional 7-coordinate intermediates is also unlikely. Indeed, recent preliminary studies on $[PtCl_6]^{2-}$ in enriched $Na^{35}Cl$ solution suggest that $Cl^-$ exchange is slow on the NMR time-scale.[62]

It thus appears that the isotopomers of the hydroxido species have chemical shifts too close to be resolved. For complex **4**, for example, the isotopomers of each isotopologue grouped together here as (B,C), (D,E,F), (G,H,I), and (J,K) should have essentially the same $^{195}$Pt shielding. This would imply that all of the data points B,C should fall on the same point, the same with D,E,F, G,H,I, and J,K. However, this is not the case neither for the pristine complex in the gas phase, where the computed spread within a group can exceed 0.5 ppm (e.g., D−F in Figure 4a), nor for the microsolvated complex, where in fact the variations between isotopomers are even greater (e.g., to ca. 1.5 ppm for G−I in Figure S7, Supporting Information).

The computed bond-length changes upon isotopic substitution ($\Delta r_g^0$ in eq 2) do not appear to be less pronounced for the hydroxido than for the aquo isotopomers. Could the variability in the shielding/bond-length derivatives be used to rationalize the different spread of the isotopomer shifts? For the prototypical complexes **2** and **5**, the $\partial\sigma_{Pt}/\partial r_{PtX}$ values are collected in Table 1. For the aquo complex **2**, those for the equatorial and axial Pt−Cl bonds (i.e., cis and trans, respectively, to $H_2O$) differ appreciably, by ca. 1800 ppm/Å. Thus, comparable bond-length changes upon isotopic substitution in these positions can translate into noticeable shift differences, and cis/trans isotopomers, that is, (B,C), (D,E,F) etc., can be resolved. Conversely, one would expect more similar shielding/bond-length derivatives for the hydroxido-complexes. However, in the gas phase, the $\partial\sigma_{Pt}/\partial r_{PtCl}$ values for the pristine hydroxido species **5** are even more disparate,


dx.doi.org/10.1021/jp405453c | J. Phys. Chem. A 2013, 117, 8054−8064

**Table 1. Shielding/Bond-Length Derivatives $\partial\sigma_{Pt}/\partial r_{PtX}$ Evaluated at the ZORA-SO/PW91 Level**

| | | $\partial\sigma_{Pt}/\partial r_{PtX}$ [ppm/Å] | |
|---|---|---|---|
| compd | bond[a] | gas phase | COSMO |
| **2** | $Pt-OH_2$ | −3136 | −3136 |
| | $Pt-Cl_{ax}$ | −2099 | −2370 |
| | $Pt-Cl_{eq}$[b] | −3885 | −4069 |
| **5** | $(r_c)Pt-OH$ | −2134 | −1978 |
| | $(r_a)Pt-Cl$ | −5188 | −4019 |
| | $(r_b)Pt-Cl$[b] | −2934 | −2962 |

[a]See Figures 1 and 5 for definition. [b]Trans to hydroxido/water ligand.

differing by more than 2000 ppm/Å for the Pt−Cl bonds cis and trans to OH ($r_a$ and $r_b$ values in Table 1). When the shielding/bond-length derivatives are evaluated in the polarizable continuum, most $\partial\sigma_{Pt}/\partial r_{PtX}$ values do not change much from the gas-phase data (compare gas-phase and COSMO entries in Table 1), with the notable exception of $r_a$ in **5**, for which this quantity decreases significantly, by more than 1000 ppm/Å. As a consequence, the $\partial\sigma_{Pt}/\partial r_{PtCl}$ values for the two different Pt−Cl bond types are now more similar for **5**, differing by little over 1000 ppm/Å. In contrast, the much larger distinction between these bonds is preserved for **2** also in the continuum.[63]

To probe whether the attenuated sensitivity of the $^{195}$Pt shieldings toward the Pt−Cl distances in the continuum would indeed translate into an improved description of the isotope shifts, we have used the COSMO shielding/bond-length derivatives from Table 1 together with the gas-phase zero-point corrections for the isotopologues and isotopomers of **5** to estimate the shieldings according to the increment method by eq 2. The result is plotted in Figure 11 along with the gas-phase

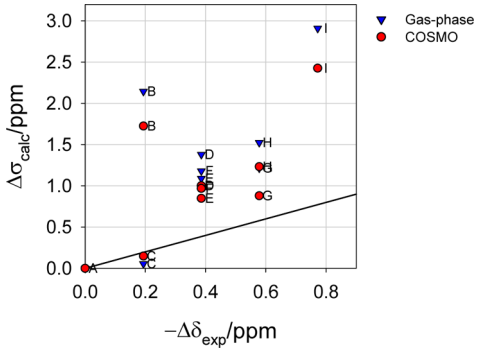


**Figure 11.** Shielding differences in $^{35/37}$Cl isotopomers of **5**, estimated from eq 2, using $\partial\sigma_{Pt}/\partial r_{PtX,I}$ in a polarizable continuum and calculated shielding differences versus negative experimental $^{35/37}$Cl isotope shifts of the isotopomers of **5**, including the line with unity slope.

shieldings calculated using DFT. Despite some scatter, the estimated shieldings are closer to the experimental observations.[12] Moreover, the near-degenerate isotopomers D, E, and F are much closer together than in the pure gas-phase DFT calculations. From these results, it seems that if the shielding/bond-length derivatives of the Pt−Cl bonds trans to the $OH^-$ or $H_2O$ are sufficiently larger than for the other Pt−Cl bonds and the averaged bond-displacements of the isotopomers are sufficiently dissimilar, then isotopomers may be resolved.

Unfortunately, the same "mixed" increment method to estimate shieldings from the gas-phase bond displacements and shielding/bond-length derivatives determined in a polarized continuum does not improve the results in general, possibly because in some cases bond-length changes can be the decisive factor, rather than the shielding/bond-length derivatives.

For the *fac*-$[PtCl_3(OH_2)_3]^+$ species **3**, for instance, immersion in a polar solvent by means of the PCM method shortens the Pt−O bond by 0.034 Å, consistent with a stronger stiffer bond. This causes the Pt−Cl bond length to increase by 0.013 Å (similar trends are found for the neutral Rh congener **11**). The effect is less pronounced in the *fac*-$[Pt^{35/37}Cl_3(OH)_3]^{2-}$ species, where the Pt−O bond length decreased by only 0.002 Å. Interestingly, the Pt−Cl bond length also decreased, by 0.029 Å. Thus, for both aquo and hydroxido complexes, there appear to be differential solvation effects on the strengths of the various bonds within a complex, which may be critical for the bond displacements in the isotopologues and isotopomers. Further theoretical work is necessary to describe these solvation effects properly and to compute and predict the isotope effects accurately.

## 4. CONCLUSIONS

We have presented calculations of magnetic shieldings at appropriate DFT levels for the isotopologues and isotopomers of a series of Pt(IV) and Rh(III) complexes obtained from $^{35/37}$Cl or $^{16/18}$O substitution of chlorido, aquo and hydroxido ligands. In most cases, the $^{195}$Pt and $^{103}$Rh NMR nuclear shieldings computed for zero-point vibrationally averages structures of these species reproduce the order of magnitude of the observed isotope shifts reasonably well, up to ca. 1 ppm, although occasionally a significant overestimation of the effects is found.

In most cases, general trends are also captured qualitatively, thus providing a theoretical basis for the origin of subtle isotope shifts in $^{195}$Pt and $^{103}$Rh NMR spectra. NMR was shown to be able to detect bond-length changes upon isotopic substitution on the femtometer scale. The computed isotope shifts can be traced back to bond-length changes via an increment method.

It has been shown that the hydroxido ligands can rotate spontaneous and rapidly (on the NMR time-scale) about the M−O bond by investigating the interconversion of two degenerate Pt(IV) rotamers, indicating that observed chemical shifts are essentially averaged between rotamers.

Agreement with experiment tends to decrease with increasing charge on the complex, and from $^{35/37}$Cl to $^{16/18}$O isotope shifts. Neglect of solvation appears to be the critical factor. For the Rh complexes, the error inherent from the neglect of the solvent in the computational protocol is inflated by the higher (relative to Pt(IV)) sensitivity toward isotopic substitution seen by the shielding/bond-length derivatives calculated for these complexes.

A possible explanation is proposed to rationalize why $^{35/37}$Cl isotopomers are not detected experimentally in some cases, notably for the Pt hydroxido-complexes. Using continuum models to calculate solvent effects on shielding/bond-length derivatives, it appears that in the aquo complexes, the sensitivity of the metal shielding toward elongation of a Pt−Cl bond strongly depends on the nature of the ligand trans to that bond (i.e., Cl or $H_2O$). In this case, certain isotopomers can be resolved experimentally. For the hydroxido-complexes, this sensivity of the metal shielding toward the individual Pt−Cl bonds is much attenuated, to the point that the latter can become magnetically equivalent. Unfortunately, neither simple polarizable continuum models nor small, microsolvated


dx.doi.org/10.1021/jp405453c | J. Phys. Chem. A 2013, 117, 8054−8064

complexes lead to generally improved isotope shifts for the series investigated.

The relativistic treatment of heavy nuclei and the addition of zero-point corrections have enhanced the use of NMR, rendering it a powerful structural tool. Often candidates differing in constitution or conformation can be distinguished on the basis of the accord between computed and experimental chemical shifts.[64] Now, theoretical modeling of structural effects on NMR parameters extends to the smallest scale, distance changes of a few femtometers upon isotopic substitution.

## ■ ASSOCIATED CONTENT

### Supporting Information

Plots of calculated $\sigma$ values vs the corresponding difference between the experimental $\delta$ values, calculated shielding differences vs negative experimental isotope shifts, shielding differences, and optimized structures. Tables of bond lengths, differences between effective and equilibrium bond lengths, and differences between effective bond distances, chemical shifts and isotopic shielding constants, and shielding/bond-length derivatives. Full refs 43 and 46. This material is available free of charge via the Internet at http://pubs.acs.org.

## ■ AUTHOR INFORMATION

### Corresponding Author

*Fax: (+44)(0)1334 463808 (M.B.); (+27)(0) 808 3342 (K.R.K.). E-mail: buehl@st-andrews.ac.uk (M.B.); krk@sun.ac.za (K.R.K.).

### Notes

The authors declare no competing financial interest.

## ■ ACKNOWLEDGMENTS

This work was supported by the School of Chemistry in St. Andrews and by EaStChem via the EaStChem Research Computing facility and a local Opteron PC cluster maintained by Dr. H. Früchtl. We gratefully acknowledge financial support from Stellenbosch University as well as Angloplatinum Ltd.

## ■ REFERENCES

(1) Pregosin, P. S. *Transition Metal Nuclear Magnetic Resonance*; Elsevier: Amsterdam, 1991.

(2) Priqueler, J. R. L.; Butler, I. S.; Rochon, F. D. An Overview of $^{195}$Pt Nuclear Magnetic Resonance Spectroscopy. *Appl. Spectrosc. Rev.* **2006**, *41*, 185−226.

(3) Still, B. M.; Kumar, P. G. A.; Aldrich-Wright, J. R.; Price, W. S. $^{195}$Pt NMR-Theory and Application. *Chem. Soc. Rev.* **2007**, *36*, 665−686.

(4) McFarlane, H. C. E.; McFarlane, W.; Rycroft, D. S. Studies of Tungsten-183 Magnetic Shielding by Heteronuclear Magnetic Double and Triple Resonance. *J. Chem. Soc., Dalton Trans.* **1976**, 1616−1622.

(5) Bendall, M.; Doddrell, D. Proton-deuterium Isotope Shifts in $^{59}$Co NMR. *Aust. J. Chem.* **1978**, *31*, 1141−1143.

(6) Naumann, F.; Rehder, D.; Pank, V. Carbonylniobium Chemistry: III. Tricarbonyl-$\eta^5$-cyclopentadienylhydridoniobate(−I): Preparation and $^{93}$Nb NMR Spectroscopic Invesitgation of $[Et_4N][CpNb(H)(CO)_3]$ and $[Et_4N][CpNb(D)(CO)_3]$. *J. Organomet. Chem.* **1982**, *240*, 363−369.

(7) Hoch, M.; Rehder, D. Isotope Effects and Coupling Constants in $[CpV\text{-}(CO)_3(^{1,2}H)]^-$ and the $^{13}$CO and C$^{18}$O Isotopomers of $CpV(CO)_4$ and $[V(CO)_6]^-$. *Inorg. Chim. Acta* **1986**, *111*, L13−L15.

(8) Jameson, C. J.; Osten, H.-J. Theoretical Aspects of Isotope Effects on Nuclear Shielding. *Annu. Rep. NMR Spectrosc.* **1986**, *17*, 1−78.

(9) Groening, O.; Elding, L. I. Water Exchange of Trans-dichlorodiaquaplatinum(II) and Tetraaquaplatinum(II) Studied by an Oxidative-addition Quenching Technique. Isotopic Shifts and Platinum-195 NMR Chemical Shifts for Mixed Chloro-aqua Complexes of Platinum(II) and Platinum(IV). *Inorg. Chem.* **1989**, *28*, 3366−3372.

(10) Ismail, I. M.; Kerrison, S. J. S.; Sadler, P. J. Chlorine and Bromine Isotope Shifts in $^{195}$Pt NMR Spectra. *J. Chem. Soc., Chem. Commun.* **1980**, *23*, 1175−1176.

(11) Gerber, W. J.; Murray, P.; Koch, K. R. $^{195}$Pt NMR Isotopologue and Isotopomer Distributions of $[PtCl_n(H_2O)_{6-n}]^{4-n}$ ($n$ = 6,5,4) Species as a Fingerprint for Unambiguous Assignment of Isotopic Stereoisomers. *Dalton Trans.* **2008**, *31*, 4113−4117.

(12) Engelbrecht, L. A. A Study of Isotope-effects in High-resolution $^{195}$Pt NMR Spectra of Octahedral Complexes of the Type $[PtCl_{6-n}(OH)_n]^{2-}$, $n$ = 0−6, in Water. M.Sc. thesis, Stellenbosch, 2013.

(13) Jameson, C. J.; Jameson, A. K. Rovibrational Averaging of Nuclear Shielding in $MX_6$-type Molecules. *J. Chem. Phys.* **1986**, *85*, 5484−5492.

(14) Jameson, C. J.; Jameson, A. K.; Oppusunggu, D. Temperature Dependence of $^{77}$Se, $^{125}$Te, and $^{19}$F Shielding and M-induced $^{19}$F Isotope Shifts in $MF_6$ Molecules. *J. Chem. Phys.* **1986**, *85*, 5480−5483.

(15) Jameson, C. J.; Rehder, D.; Hoch, M. Isotope and Temperature Dependence of Transition-metal Shielding in Complexes of the Type $M(XY)_6$. *J. Am. Chem. Soc.* **1987**, *109*, 2589−2594.

(16) Murray, P.; Gerber, W. J.; Koch, K. R. $^{35/37}$Cl and $^{16/18}$O Isotope Resolved $^{195}$Pt NMR: Unique Spectroscopic "Fingerprints" for Unambiguous Speciation of $[PtCl_n\ (H_2O)\ _{6-n}]^{4-n}$ ($n$= 2−5) Complexes in an Acidic Aqueous Solution. *Dalton Trans.* **2012**, *41*, 10533−10542.

(17) Bühl, M. DFT Computations of Transition-Metal Chemical Shifts. *Annu. Rep. NMR Spectrosc.* **2008**, *64*, 77−126.

(18) Autschbach, J.; Le Guennic, B. Solvent Effects on $^{195}$Pt and $^{205}$Tl NMR Chemical Shifts of the Complexes $[(NC)_5Pt\text{-}Tl(CN)_n]^{n-}$ ($n$ = 0−3), and $[(NC)_5Pt\text{-}Tl\text{-}Pt(CN)_5]^{3-}$ Studied by Relativistic Density Functional Theory. *Chem.-Eur. J.* **2004**, *10*, 2581−2589.

(19) Sterzel, M.; Autschbach, J. Toward an Accurate Determination of $^{195}$Pt Chemical Shifts by Density Functional Computations: The Importance of Unspecific Solvent Effects and the Dependence of Pt Magnetic Shielding Constants on Structural Parameters. *Inorg. Chem.* **2006**, *45*, 3316−3324.

(20) Autschbach, J.; Zheng, S. H. Analyzing Pt Chemical Shifts Calculated from Relativistic Density Functional Theory Using Localized Orbitals: The Role of Pt 5d Lone Pairs. *Magn. Reson. Chem.* **2008**, *46*, S45−S55.

(21) Grigoleit, S.; Bühl, M. Computational $^{59}$Co NMR Spectroscopy: Beyond Static Molecules. *J. Chem. Theory Comput.* **2005**, *1*, 181−193.

(22) Bühl, M.; Grigoleit, S.; Kabrede, H.; Mauschick, F. T. Simulation of $^{59}$Co NMR Chemical Shifts in Aqueous Solution. *Chem.-Eur. J.* **2006**, *12*, 477−488.

(23) Koch, K. R.; Burger, M. R.; Kramer, J.; Westra, A. N. $^{195}$ Pt NMR and DFT Computational Methods as Tools Towards the Understanding of Speciation and Hydration/Solvation of $[PtX_6]^{2-}$ (X = $Cl^-$, $Br^-$) Anions in Solution. *Dalton Trans.* **2006**, 3277−3284.

(24) Davis, J. C.; Bühl, M.; Koch, K. R. On the Origin of $^{35/37}$Cl Isotope Effects on $^{195}$Pt NMR Chemical Shifts. A Density Functional Study. *J. Chem. Theory Comput.* **2012**, *8*, 1344−1350.

(25) Bühl, M.; Sieffert, N.; Chaumont, A.; Wipff, G. Water versus Acetonitrile Coordination to Uranyl. Density Functional Study of Cooperative Polarization Effects in Solution. *Inorg. Chem.* **2011**, *50*, 299−308.

(26) See, for instance: Rotzinger, F. R. Performance of Molecular Orbital Methods and Density Functional Theory in the Computation of Geometries and Energies of Metal Aqua Ions. *J. Phys. Chem. B* **2005**, *109*, 1510−1527.

(27) Ernsting, J. M.; Gaemers, S.; Elsevier, C. J. $^{103}$Rh NMR Spectroscopy and Its Application to Rhodium Chemistry. *Magn. Reson. Chem.* **2004**, *42*, 721−736.

(28) Geswindt, T. E.; Gerber, W. J.; Brand, D. J.; Koch, K. R. $^{35}Cl/^{37}Cl$ Isotope Effects in $^{103}Rh$ NMR of $[RhCl_n(H_2O)_{6-n}]^{3-n}$ Complex Anions in Hydrochloric Acid Solution as a Unique 'NMR finger-print' for Unambiguous Speciation. *Anal. Chim. Acta* **2012**, *730*, 93−98.
(29) Perdew, J. P.; Burke, K.; Ernzerhof, M. Generalized Gradient Approximation Made Simple. *Phys. Rev. Lett.* **1996**, *77*, 3865−3868.
(30) Adamo, C.; Barone, V. Toward Reliable Density Functional Methods Without Adjustable Parameters: The PBE0Model. *J. Chem. Phys.* **1999**, *110*, 6158−6170.
(31) Dolg, M.; Wedig, U.; Stoll, H.; Preuss, H. Energy-adjusted Ab Initio Pseudopotentials for the First Row Transition Elements. *J. Chem. Phys.* **1987**, *86*, 866−873.
(32) Ditchfield, R.; Hehre, W. J.; Pople, J. A. Self-Consistent Molecular-Orbital Methods. IX. An Extended Gaussian-Type Basis for Molecular-Orbital Studies of Organic Molecules. *J. Chem. Phys.* **1971**, *54*, 724−728.
(33) Hehre, W. J.; Ditchfield, R.; Pople, J. A. Self-Consistent Molecular Orbital Methods. XII. Further Extensions of Gaussian-Type Basis Sets for Use in Molecular Orbital Studies of Organic Molecules. *J. Chem. Phys.* **1972**, *56*, 2257−2261.
(34) Hariharan, P. C.; Pople, J. A. The Influence of Polarization Functions on Molecular Orbital Hydrogenation Energies. *Theor. Chim. Acta* **1973**, *28*, 213−222.
(35) Bühl, M.; Reimann, C.; Pantazis, D. A.; Bredow, T.; Neese, F. Geometries of Third-Row Transition-Metal Complexes from Density-Functional Theory. *J. Chem. Theory Comput.* **2008**, *4*, 1449−1459.
(36) Barone, V. Anharmonic Vibrational Properties by a Fully Automated Second-order Perturbative Approach. *J. Chem. Phys.* **2005**, *122*, 014108.1−014108.10.
(37) Barone, V. Vibrational Zero-point Energies and Thermodynamic Functions Beyond the Harmonic Approximation. *J. Chem. Phys.* **2004**, *120*, 3059−3065.
(38) Ruud, K.; Åstrand, P. O.; Taylor, P. R. An Efficient Approach for Calculating Vibrational Wave Functions and Zero-point Vibrational Corrections to Molecular Properties of Polyatomic Molecules. *J. Chem. Phys.* **2000**, *112*, 2668−2684.
(39) Ruud, K.; Åstrand, P. O.; Taylor, P. R. Zero-point Vibrational Effects on Proton Shieldings: Functional-group Contributions from Ab Initio Calculations. *J. Am. Chem. Soc.* **2001**, *123*, 4826−4833.
(40) Ruden, T.; Lutnæss, O. B.; Helgaker, T. Vibrational Corrections to Indirect Nuclear Spin−spin Coupling Constants Calculated by Density-functional Theory. *J. Chem. Phys.* **2003**, *118*, 9572−9581.
(41) The formalism used in this study is in lowest order equivalent to one where the NMR shielding constants and their derivatives are calculated at the equilibrium geometry and the vibrational corrections are obtained from a two-term equation. For an application of the latter, see, for example, ref 42. For zero-point corrections, the effective-geometry method is simpler, but if one would be interested in the temperature dependence of the vibrational corrections, the two-term equation is more economic to use.
(42) Mort, B. C.; Autschbach, J. Zero-point Corrections and Temperature Dependence of HD Spin-spin Coupling Constants of Heavy Metal Hydride and Dihydrogen Complexes Calculated by Vibrational Averaging. *J. Am. Chem. Soc.* **2006**, *128*, 10060−10072.
(43) Frisch, M. J.; et al. *Gaussian 09*; Gaussian, Inc.: Pittsburgh, PA, 2009. See the Supporting Information for the full reference.
(44) Perdew, J. P.; Wang, Y. Accurate and Simple Analytic Representation of the Electron-gas Correlation Energy. *Phys. Rev. B* **1992**, *45*, 13244−13249.
(45) Perdew, J. P. Unified Theory of Exchange and Correlation Beyond the Local Density Approximation. In *Electronic Structure of Solids '91*; Ziesche, P., Eschrig, H., Eds.; Akademie Verlag: Berlin, 1991; pp 11−20.
(46) Baerends, E. J.; et al. *ADF2010*. See the Supporting Information for the full reference.
(47) Barone, V.; Cossi, M. Quantum Calculation of Molecular Energies and Energy Gradients in Solution by a Conductor Solvent Model. *J. Phys. Chem. A* **1998**, *102*, 1995−2001.
(48) Cossi, M.; Rega, N.; Scalmani, G.; Barone, V. Energies, Structures, and Electronic Properties of Molecules in Solution with the C-PCM Solvation Model. *J. Comput. Chem.* **2003**, *24*, 669−681.
(49) Pye, C. C.; Ziegler, T. An Implementation of the Conductor-like Screening Model of Solvation within the Amsterdam Density Functional Package. *Theor. Chem. Acc.* **1999**, *101*, 396−408.
(50) Burger, M. R.; Kramer, J.; Chermette, H.; Koch, K. R. A Comparison of Experimental and DFT Calculations of $^{195}Pt$ NMR Shielding Trends for $[PtX_nY_{6-n}]^{2-}$ (X, Y = Cl, Br, F and I) Anions. *Magn. Reson. Chem.* **2010**, *48*, S38−S47.
(51) Pyykko, P. Relativistic Effects in Structural Chemistry. *Chem. Rev.* **1988**, *88*, 563−594.
(52) Orian, L.; Bisello, A.; Santi, S.; Ceccon, A.; Saielli, G. $^{103}Rh$ NMR Chemical Shifts in Organometallic Complexes: A Combined Experimental and Density Functional Study. *Chem.-Eur. J.* **2004**, *10*, 4029−4040.
(53) Bondar, V. I.; Potekhin, K. A.; Rau, T. F.; Rozman, S. P.; Rau, V. G.; Struchkov, Y. T. Crystal Structure of $[Cr(OCN_2H_4)_6]$ $[Pt(OH)Cl_5]$ $(ClO_4)$ $H_2O$. *Sov. Phys. Dokl.* **1988**, *33*, 395.
(54) Murray, P.; Koch, K. R. A $^{195}Pt$ NMR Study of the Oxidation of $[PtCl_4]^{2-}$ with Chlorate, Bromate, and Hydrogen Peroxide in Acidic Aqueous Solution. *J. Coord. Chem.* **2010**, *63*, 2561−2577.
(55) Elder, R. C.; Heeg, M. J.; Payne, M. D.; Trkula, M.; Deutsch, E. Trans Effect in Octahedral Complexes. 3. Comparison of Kinetic and Structural Trans Effects Induced by Coordinated Sulfur in Sulfito- and Sulfinatopentaaminecobalt(III) Complexes. *Inorg. Chem.* **1978**, *17*, 431−440.
(56) Keeler, J. *Understanding NMR Spectroscopy*; Wiley: New York, 2011.
(57) Wagner, C.; Bruhn, C.; Gravenhorst, O.; Steinborn, D. Structure and Vibrational Spectra of *cis*-diaquatetra-chloroplatinum (IV)-(18-crown-6)-water (1/1/2), cis-$[PtCl_4$ $(H_2O)$ $_2]$.(18-cr-6)·$2H_2O$. *Z. Kristallogr.* **2000**, *215*, 61−64.
(58) Both the trans and the cis isomers of $[RhCl_4(H_2O)_2]^-$ (see Figure S6, Supporting Information) are found as stable crystals as indicated by the XRD data in Table S9 of the Supporting Information. The calculated energies for both differ by a mere 0.002 kcal/mol; however, for consistency with the $^{195}Pt$ system in this study, only the cis isomer, **10**, is used in the calculation of isotope shifts.
(59) For first-principles molecular dynamics simulations of $^{195}Pt$ NMR chemical shifts in solution, see, for example, refs 60 and 61. We note that such MD simulations with classical propagation of the nuclei are mass-dependent and should thus, in principle, be capable of describing isotope effects on nuclear shieldings. No quantum (i.e., zero-point) effects would be included, however, and it would appear doubtful whether the simulations could be converged to the high numerical precision required for the minute effects we are trying to model.
(60) Truflandier, L. A.; Autschbach, J. Probing the Solvent Shell with $^{195}Pt$ Chemical Shifts: Density Functional Theory Molecular Dynamics Study of Pt-II and Pt-IV Anionic Complexes in Aqueous Solution. *J. Am. Chem. Soc.* **2010**, *132*, 3472−3483.
(61) Truflandier, L. A.; Sutter, K.; Autschbach, J. Solvent Effects and Dynamic Averaging of $^{195}Pt$ NMR Shielding in Cisplatin Derivatives. *Inorg. Chem.* **2011**, 1723−1732.
(62) Murray, P. A speciation study of various Pt(II) and Pt(IV) complexes including hexaaquaplatinum(IV) by means of $^{195}Pt$ NMR spectroscopy, in support of a preliminary study of the oxidation mechanism of various Pt(II) complexes. *Ph.D. thesis*, Stellenbosch, 2013.
(63) For the Rh aquo complex **10**, the shielding/bond-length derivatives are very similar in the gas phase and the continuum; see Figure S5 in the Supporting Information.
(64) Bühl, M.; van Mourik, T. NMR Spectroscopy: Quantum-chemical Calculations. *WIREs Comput. Mol. Sci.* **2011**, *1*, 634−647.